Integration of CFD and EFD for Analysis of Complex Real Flows

Toshiyuki Hayase

Institute of Fluid Science
Tohoku University
Sendai, 980-8577
Japan
Hayase@ifs.tohoku.ac.jp

Abstract

In this article formulation of MI simulation and equations of linearized error dynamics and eigenvalue analysis of MI simulation were first explained. Example of MI simulation was presented for a fully developed turbulent flow in a square duct. Numerical experiment was performed for MI simulation with a feedback signal from the predetermined standard turbulent flow solution. Convergence of MI simulation to the standard solution was investigated as a function of feedback gain and spatial and temporal density of feedback signal. Eigenvalue analysis was performed to examine the validity of the linearized error dynamics approach in the design of feedback signal.

Key words: measurement-integrated simulation, turbulent flow, eigenvalue analysis, convergence.

Introduction

Recent advances in computational fluid dynamics enable calculation of complex flows including turbulent flows appearing in many practical applications with reasonable accuracy. However, an *accurate solution* usually does not mean a solution that reproduces the exact instantaneous structure of the real flow, but rather one having the same statistical characteristics as those of the relevant flow. It is quite difficult to obtain the exact turbulent flow solution because (1) it is difficult to specify the initial and/or boundary conditions of real turbulent flows correctly, and (2) even if these data are available, a very small error in the initial condition will increase exponentially in structurally unstable dynamical systems such as turbulent flows [1] (see Fig. 1).
In spite of the inherent difficulty, reproducing the exact structure of real turbulent flows is a critically important issue in many fields, such as weather forecasting or feedback flow control. Extensive studies have been carried out to obtain information on real flows, including turbulent flows. Assimilation is a method commonly used in numerical weather prediction [2]. In a numerical simulation to calculate future weather states, the initial condition is updated at every time interval using the latest computational result and the measurement data around the computational grid points. 4 Dimensional variation (4DVAR) is widely used in numerical weather forecasting [3-5], but it requires huge computational power to repeatedly solve flow dynamics and its adjoint, and, therefore, is not suitable to apply to problems of real-time flow reproduction such as feedback flow control.

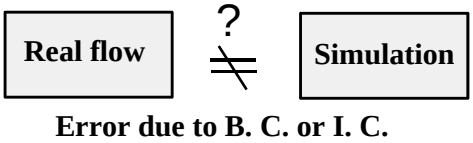

Fig.1 Real flow and simulation.

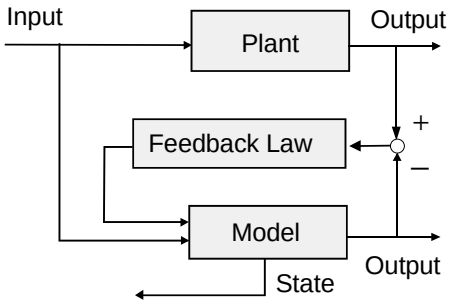

Fig.2 Block diagram of observer.

A similar concept, namely, interactive computational-experimental methodology (ICEME), was proposed by Humphrey [6] for application to engineering problems, in which the measurement data is supplied to a thermal-flow simulation to enhance the efficiency of computation. Possible advantages of ICEME as well as further necessary studies were discussed in relation to a complex flow related optimization problem seeking the arrangement of electrical heat sources to minimize the temperature in a ventilated box under some constraints. At that time, however, little was known as to how computational and experimental methods should be integrated in general to obtain useful information on the flow. Zeldin and Meade applied Tikhonov regularization method, which is common in inverse problems, to obtain an optimum solution to estimate the real flow from the numerical and measurement results of the relevant flow [7]. Particle imaging velocimetry has become a mature method to obtain velocity vectors in a flow domain. Studies have been made on the application of CFD schemes to modify PIV measurement so as to satisfy physical constraints such as the continuity equation [8]. State estimator or observer, which is fundamental methodology in modern control theory to estimate the state variables from the state equation with the aid of partial measurement data, has been used in flow problems. Uchiyama and Hakomori [9] reproduced the unsteady flow field in a pipe using a Kalman filter, which is a special observer [10]. Recently, Högberg *et al*. constructed a Kalman filter to estimate the flow state from the information on the wall in a numerical experiment for the optimum control of the subcritical instability of a channel flow based on a linearized equation [11]. Kalman filter and observer seek the asymptotic convergence to the optimum state requiring only one forward integration from arbitrary initial condition. They are potential candidates to solve the problem to reproduce real flows due to much less computational load than the variational methods. By comparing Kalman filter and observer, the latter has a simpler structure retaining essential part of the state estimation. One of the present authors proposed a measurement-integrated simulation (hereafter abbreviated as “MI simulation”), which is a kind of observer using a CFD scheme as the mathematical model of a relevant system, and successfully applied it to a turbulent flow in a square duct [12], a Karman vortex street behind a square cylinder [13, 14], and blood flow in an aneurismal aorta [15].

Among these studies intending to reproduce real flows, none has been successful in exactly reproducing instantaneous structures of a turbulent flow. From both theoretical and practical points of view, it is interesting to examine if any of these methods is capable of exactly reproducing turbulent flows using partial measurement data. As mentioned above, 4DVAR may be a sophisticated way to solve the problem but is practically inappropriate due to its large computational load. The present paper deals with this problem for MI simulation considering a low computational load and an accurate physical model.

Table 1 Comparison among observer-based methods.

	Model	Feedback design
Observer	**Linear ordinary differential equation**	**Pole placement**
Kalman filter	**Linear ordinary differential equation**	**Optimum design**
MI simulation	**CFD model**	**Trial and error**

As mentioned above, MI simulation is a kind of observer. In the following we give a general explanation of observers and show the differences between the MI simulation and other existing observers, including the Kalman filter. An observer is a common tool in control theory to estimate the real state from a mathematical model and partial measurement [13]. As shown in the block diagram in Fig. 2, the real system ("Plant" in the figure) is modeled as a differential equation ("Model"). Real time computation is performed parallel to the measurement, and the difference between the outputs of the computation and measurement, or the estimation error, is fed back to the model through the feedback law. This feedback signal modifies the dynamical structure of the model system and the properly designed feedback law results in an asymptotic reduction of the estimation error. In observable linear systems, convergence of the output signal guarantees coincidence of all state variables [16]. In design of the observer, determination of the mathematical model and that of the feedback law are the key (see Table 1). For finite dimensional linear dynamical systems satisfying observability condition, the observer of an arbitrary exponential convergence property can be designed by the standard pole placement technique [16]. A Kalman filter is also a kind of observer in which the feedback gain is determined to minimize the cost function in consideration of the statistical behavior of the measurement in stochastic dynamical systems [10]. Extension of the observer for application to nonlinear systems has been studied extensively for finite dimensional cases [17]. For infinite dimensional linear systems, the state observer is designed in the same manner as in finite dimensional cases and implemented after finite-dimensional approximation [18]. However, a general theory of the observer applicable to infinite dimensional and nonlinear dynamical systems such as flows has not yet been established [19]. As a methodology to reproduce real flows, the authors have proposed an MI simulation. The main feature of the MI simulation, which distinguishes it from other existing observers, is usage of CFD scheme as a mathematical model of the physical flow. A large dimensional nonlinear CFD model makes it difficult to design the feedback law in a theoretical manner; therefore, it has been determined by a trial and error method based on physical considerations. However, it makes it possible to accurately reproduce real flows once the feedback law is properly designed.

In this article formulation of MI simulation and equations of linearized error dynamics and eigenvalue analysis of MI simulation are explained [20]. Example of MI simulation is presented for a fully developed turbulent flow in a square duct. Numerical experiment is performed for MI simulation with a feedback signal from the predetermined standard turbulent flow solution [21]. Convergence of MI simulation to the standard solution is investigated as a function of feedback gain and spatial and temporal density of feedback signal. Eigenvalue analysis is performed to examine the validity of the linearized error dynamics approach in the design of feedback signal [20].

Measurement Integrated Simulation

In this section formulation of MI simulation and equations of linearized error dynamics and eigenvalue analysis of MI simulation are explained [20].

Formulation

This paper deals with incompressible and viscous fluid flow. The dynamic behavior of the flow field is governed by the Navier-Stokes equation:

$$\frac{\partial \mathbf{u}}{\partial t} = -\left(\mathbf{u}\cdot\nabla\right)\mathbf{u} + \nu\cdot\Delta\mathbf{u} - \nabla p + \mathbf{f} \tag{1}$$

and the equation of mass continuity:

$$\nabla\mathbf{u} = 0 \tag{2}$$

as well as by the initial and the boundary conditions. In the Navier-Stokes equation (1), $\mathbf{f}$ denotes the external force term as the feedback signal in the MI simulation, $\rho\mathbf{f}$ denotes the body force, and p denotes pressure divided by density. The pressure equation is derived from Eqs. (1) and (2) as

$$\Delta p = -\mathrm{div}\left\{\left(\mathbf{u}\cdot\nabla\right)\mathbf{u}\right\} + \nabla\mathbf{f} \tag{3}$$

We use Eqs. (1) and (3) as the fundamental equations. In the following, Eqs. (1) and (3) are simplified as Eqs. (4).

$$\begin{cases} \dfrac{\partial \mathbf{u}}{\partial t} = \mathbf{g}(\mathbf{u}) - \nabla p + \mathbf{f} \\ \Delta p = q(\mathbf{u}) + \nabla \mathbf{f} \end{cases} \tag{4}$$

where

$$\begin{cases} \mathbf{g}(\mathbf{u}) = -(\mathbf{u}\cdot\nabla)\mathbf{u} + \nu\cdot\Delta\mathbf{u} \\ q(\mathbf{u}) = -\mathrm{div}\{(\mathbf{u}\cdot\nabla)\mathbf{u}\} \end{cases} \tag{5}$$

The basic equation of the numerical simulation is represented as a spatially discretized form of governing equations (4):

$$\begin{cases} \dfrac{d\mathbf{u}_N}{dt} = \mathbf{g}_N(\mathbf{u}_N) - \nabla_N \mathbf{p}_N + \mathbf{f}_N \\ \Delta_N \mathbf{p}_N = \mathbf{q}_N(\mathbf{u}_N) + \nabla_N{}^T \mathbf{f}_N \end{cases} \tag{6}$$

where $\mathbf{u}_N$ and $\mathbf{p}_N$ are computational results for the $3N$-dimensional velocity vector and the N-dimensional pressure vector, respectively, N denotes the number of grid points, and ∇_N and Δ_N are matrices which express the discrete form of operators ∇ and Δ. It is noted that effects of the boundary conditions are included in the functions $\mathbf{g}_N$ and $\mathbf{q}_N$.

We define the operator $\mathbf{D}_N(\bullet)$ to generate the N-dimensional vector consisting of the values of a scalar field sampled at N grid points. Definition of $\mathbf{D}_N$ is naturally extended to the case when the variable is a velocity vector field as $\mathbf{D}_N(\mathbf{u}) = \left[\mathbf{D}_N(u_1)^T \quad \mathbf{D}_N(u_2)^T \quad \mathbf{D}_N(u_3)^T\right]^T$. Applying the operator to the Navier Stokes equation and the pressure equation, we obtain the sampling of these equations at N grid points as,

$$\begin{cases} \dfrac{d}{dt}\mathbf{D}_N(\mathbf{u}) = \mathbf{D}_N(g(\mathbf{u})) - \mathbf{D}_N(\nabla p) \\ \mathbf{D}_N(\Delta p) = \mathbf{D}_N(q(\mathbf{u})) \end{cases} \tag{7}$$

We assume that there is no external force ($\mathbf{D}_N(\mathbf{f}) = 0$) in the real flow. On the other hand, we apply external force denoted by a function of real flow and numerical simulation in MI simulation. In this study, we consider the case in which external force $\mathbf{f}_N$ is denoted by a linear function of the difference of velocity and pressure between real flow and numerical simulation:

$$\mathbf{f}_N = -\mathbf{K}_u\left\{\mathbf{C}_u\mathbf{u}_N - \mathbf{C}_u\left(\mathbf{D}_N(\mathbf{u}) + \boldsymbol{\varepsilon}_u\right)\right\} - \mathbf{K}_p\left\{\mathbf{C}_p\mathbf{p}_N - \mathbf{C}_p\left(\mathbf{D}_N(p) + \boldsymbol{\varepsilon}_p\right)\right\} \tag{8}$$

where $\mathbf{K}_u$ denotes the $3N$-by-$3N$ feedback gain matrix of velocity, $\mathbf{K}_p$ denotes the $3N$-by-N feedback gain matrix of pressure, $\mathbf{C}_u$ and $\mathbf{C}_p$ denote the $3N$-by-$3N$ and N-by-N diagonal matrices consisting of diagonal elements of 1 for measurable points or 0 for immeasurable points, and $3N$-dimensional vector $\boldsymbol{\varepsilon}_u$ and N-dimensional vector $\boldsymbol{\varepsilon}_p$ mean measurement error. By introducing Eq. (8) into Eq. (6), we derive the general formulation of MI simulation:

$$\begin{cases} \dfrac{d\mathbf{u}_N}{dt} = \mathbf{g}_N(\mathbf{u}_N) - \nabla_N\mathbf{p}_N - \mathbf{K}_u\mathbf{C}_u\left\{\mathbf{u}_N - \left(\mathbf{D}_N(\mathbf{u}) + \boldsymbol{\varepsilon}_u\right)\right\} - \mathbf{K}_p\mathbf{C}_p\left\{\mathbf{p}_N - \left(\mathbf{D}_N(p) + \boldsymbol{\varepsilon}_p\right)\right\} \\ \Delta_N\mathbf{p}_N = \mathbf{q}_N(\mathbf{u}_N) - \nabla_N{}^T\mathbf{K}_u\mathbf{C}_u\left\{\mathbf{u}_N - \left(\mathbf{D}_N(\mathbf{u}) + \boldsymbol{\varepsilon}_u\right)\right\} - \nabla_N{}^T\mathbf{K}_p\mathbf{C}_p\left\{\mathbf{p}_N - \left(\mathbf{D}_N(p) + \boldsymbol{\varepsilon}_p\right)\right\} \end{cases} \tag{9}$$

Linearized error dynamics

We derive the linearized error dynamics of MI simulation. Disregarding the second order and higher order terms in Taylor expansion for the difference between real flow as Eq. (7) and the basic equation of MI simulation as Eq. (9) with respect to $\mathbf{u}_N$-$\mathbf{D}_N(\mathbf{u})$ and $\mathbf{p}_N$-$\mathbf{D}_N(p)$, we can derive the linearized error dynamics:

$$\frac{d}{dt}\left(\mathbf{u}_N-\mathbf{D}_N(\mathbf{u})\right)=\left(\left.\frac{d\mathbf{g}_N}{d\mathbf{u}_N}\right|_{\mathbf{u}_N}-\mathbf{K}_u\mathbf{C}_u\right)\left(\mathbf{u}_N-\mathbf{D}_N(\mathbf{u})\right)+\left(-\nabla_N-\mathbf{K}_p\mathbf{C}_p\right)\left(\mathbf{p}_N-\mathbf{D}_N(p)\right)$$
$$+\underline{\left\{\mathbf{g}_N\left(\mathbf{D}_N(\mathbf{u})\right)-\mathbf{D}_N\left(\mathbf{g}(\mathbf{u})\right)\right\}+\left(-\nabla_N\mathbf{D}_N(p)+\mathbf{D}_N(\nabla p)\right)}+\underline{\underline{\mathbf{K}_u\mathbf{C}_u\boldsymbol{\varepsilon}_u}} \tag{10}$$

and complementary static equation for pressure error:

$$\left(\mathbf{p}_N-\mathbf{D}_N(p)\right)=\left(\Delta_N+\nabla_N^T\mathbf{K}_p\mathbf{C}_p\right)^{-1}\left(\left.\frac{d\mathbf{q}_N}{d\mathbf{u}_N}\right|_{\mathbf{u}_N}-\nabla_N^T\mathbf{K}_u\mathbf{C}_u\right)\left(\mathbf{u}_N-\mathbf{D}_N(\mathbf{u})\right)$$
$$+\underline{\left(\Delta_N+\nabla_N^T\mathbf{K}_p\mathbf{C}_p\right)^{-1}\left\{\mathbf{g}_N\left(\mathbf{D}_N(\mathbf{u})\right)-\Delta_N\mathbf{D}_N(p)\right\}}+\underline{\underline{\left(\Delta_N+\nabla_N^T\mathbf{K}_p\mathbf{C}_p\right)^{-1}\nabla_N^T\left(\mathbf{K}_u\mathbf{C}_u\boldsymbol{\varepsilon}_u+\mathbf{K}_p\mathbf{C}_p\boldsymbol{\varepsilon}_p\right)}} \tag{11}$$

where the underlined terms are caused by the model error including that in the boundary conditions and the double-underlined terms are caused by measurement error.

Here, we derive the basic equation of eigenvalue analysis for the linearized error dynamics which are formulated as Eqs. (10) and (11) in previous section. In this paper, we consider the case of no model error including that in the boundary conditions, no measurement error, and feedback with only velocity components ($\mathbf{K}_p$=0). In this case, Eq. (10) is written as

$$\frac{d\mathbf{e}_u}{dt}=\mathbf{A}\mathbf{e}_u-\nabla_N\mathbf{e}_p \tag{12}$$

where $\mathbf{e}_u$, $\mathbf{e}_p$ and A are the difference in velocity and pressure between the MI simulation and the real flow and the $3N$-by-$3N$ matrix defined as

$$\mathbf{e}_u=\mathbf{u}_N-\mathbf{D}_N(\mathbf{u}),\quad \mathbf{e}_p=\mathbf{p}_N-\mathbf{D}_N(p),\quad \mathbf{A}=\left.\frac{d\mathbf{g}_N}{d\mathbf{u}_N}\right|_{\mathbf{u}_N}-\mathbf{K}_u\mathbf{C}_u \tag{13}$$

Next we reduce the dimension of the velocity error vector $\mathbf{e}_u$ based on the Weyl decomposition. In Weyl decomposition, any vector field $\mathbf{w}$ can be uniquely decomposed into the orthogonal vector fields $\mathbf{v}$ and grad ϕ as,

$$\mathbf{w}=\mathbf{v}+\operatorname{grad}\phi$$
$$\operatorname{div}\mathbf{v}=0\quad\text{and}\quad\mathbf{v}\cdot\mathbf{n}=0,\ \mathbf{x}\in\partial V \tag{14}$$

where $\mathbf{n}$ denotes the unit vector normal to the boundary. In the present analysis, the velocity error $\mathbf{e}_u$ consists only of $\mathbf{v}$ component in Weyl decomposition since it satisfies the divergence-free condition and it vanishes on the boundary due to the above mentioned assumption of no model error. This enables us to reduce the dimension of $\mathbf{e}_u$ corresponding to that of the component of grad ϕ.

Referring to Fig. 3, we define B as the range of ∇_N in Eq. (12),

$$\mathbf{B}=\operatorname{Range}\left(\nabla_N\right) \tag{15}$$

and $3N$-by-$2N$ matrix $\tilde{\mathrm{B}}$ consisting of $\tilde{\mathbf{b}}_1,\tilde{\mathbf{b}}_2,\cdots,\tilde{\mathbf{b}}_{2N}$ the orthonomal basis of $\mathrm{B}^{\perp}$, the orthogonal complementary space of B.

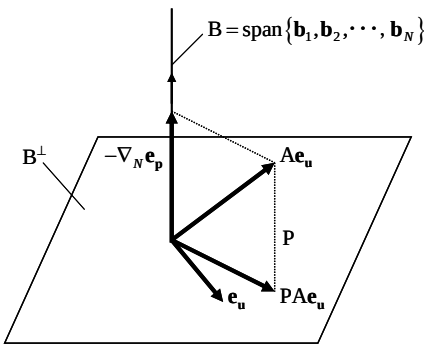

Fig. 3 Schematic Diagram for projection of vector field.

$$\tilde{\mathbf{B}} = \left[\tilde{\mathbf{b}}_1 \quad \tilde{\mathbf{b}}_2 \quad \cdots \quad \tilde{\mathbf{b}}_{2N} \right] \tag{16}$$

The projection of Eq. (12) onto $B^{\perp}$ results in the following relation.

$$\frac{d}{dt}\mathbf{e}_u{}' = \mathbf{A}'\mathbf{e}_u{}' \tag{17}$$

where the $2N$ dimensional vector $\mathbf{e}_u{}'$ and A' are given as

$$\mathbf{e}_u = \tilde{\mathbf{B}}\mathbf{e}_u{}', \quad \mathbf{A}' = \tilde{\mathbf{B}}^T \mathbf{A} \tilde{\mathbf{B}} \tag{18}$$

We can analyze the linearized error dynamics from the eigenvalues of the $2N$-by-$2N$ system matrix $\mathbf{A}'$.

Numerical Experiment for Turbulent Flow in Square Duct

In this section example of MI simulation are presented for a fully developed turbulent flow in a square duct. Numerical experiment is performed for MI simulation with a feedback signal from the predetermined standard turbulent flow solution [21]. Convergence of MI simulation to the standard solution is investigated as a function of feedback gain and spatial and temporal density of feedback signal. Next, eigenvalue analysis is performed to examine the validity of the linearized error dynamics approach in the design of feedback signal [20].

Reproduction of turbulent flow

A numerical experiment was performed to examine whether a turbulent flow structure is exactly reproduced by an MI simulation using partial information on the real flow. We consider a fully developed turbulent flow in a pipe with a square cross section, which is a typical flow case [22, 23]. In our former attempt of MI simulation for this flow, a real turbulent flow was modeled by a pre-calculated standard solution, and an ad-hoc feedback law using a limited number of data of the standard solution was derived based on a physical consideration; a pressure difference proportional to the difference in the axial flow velocity component on a specified cross section normal to the pipe axis was added to the pressure boundary condition [12]. By choosing a feedback gain, the estimation error was reduced by a factor of 0.6, but it was far from an exact reproduction of the standard solution. In the present paper, we intend to reproduce the standard solution exactly with a more general feedback law using as much information on the standard solution as available and then investigate the possibility of reducing the number of data.

In the followings, a numerical experiment is performed for a relevant flow. After validation of the numerical solution procedure, a standard turbulent flow solution is obtained as a model of a physical flow. The MI simulation is performed for the cases in which (1) all velocity components of the standard solution are available at all grid points, (2) partial velocity components are available at all grid points, and (3) all velocity components are available at partial grid points. We investigate the convergence of the MI simulation to the standard solution for these cases.

The computational scheme used in this study is the same as that of our previous study [23]. A brief explanation of the numerical scheme is presented here. The discretized representations of the Navier-Stokes equation (1) and the pressure equation (3) are obtained by the finite volume method on a three-dimensional orthogonal

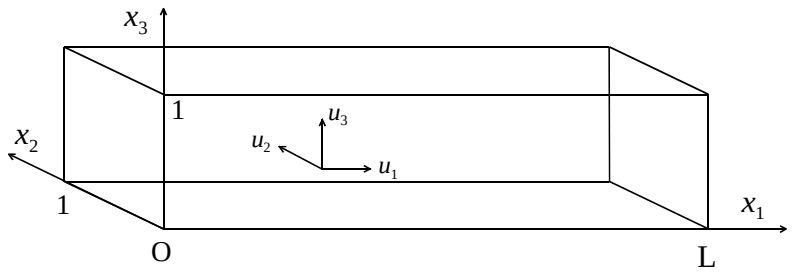

Fig. 4 Domain and coordinate system.

equidistant staggered grid system. Convection terms are discretized by the reformulated QUICK scheme, which assures the continuity of the momentum flux on the control volume boundaries in the iteration process [25]. A two-time level implicit scheme is used for time dependent terms [26]. The resultant set of finite difference equations is solved using the iterative procedure based on the SIMPLER method of Patankar [27].
The geometry and the coordinate system treated in this study are shown in Fig. 4. As to the boundary condition, the periodical velocity condition and the constant pressure difference, δ_p is assumed between the upstream and downstream boundaries, and a non-slip condition is assumed on the walls. In this paper all the values are expressed in dimensionless form using the side length of the square cross section $\tilde{b}$, the density of fluid $\tilde{\rho}$ and the mean axial velocity $\tilde{u}_{m0}$ given by

$$\tilde{u}_{m0} = \sqrt{2\tilde{\delta}_p \tilde{b} / (\lambda \tilde{L} \tilde{\rho})}, \tag{19}$$

where the coefficient of resistance λ is given by the Blasius' formula [24]

$$\lambda = 0.316 R_{e0}^{-1/4}. \tag{20}$$

A constant pressure difference $\delta_p = \tilde{\delta}_p / (\tilde{\rho} \tilde{u}_{m0}^2)$ corresponding to a specified Reynolds number $R_{e0} = \tilde{u}_{m0} \tilde{b} / \tilde{\nu}$ is assumed between the upstream and downstream boundaries for the duct of the periodical length L.

The calculations were carried out on the SGI ORIGIN 2000 and Altix 3700 Bx2 at the Institute of Fluid Science, Tohoku University. An ordinary numerical simulation was first carried out to obtain two solutions: the one solution was used as the model of a real flow (hereafter we call it ''standard solution''), and the other solution was obtained from the initial condition different from that of the standard solution (hereafter we call the solution as ''ordinary simulation''). Then MI simulation was performed from the same initial condition as that of the ordinary simulation but with the feedback signal in which the standard solution was used as the velocity of the real flow. Convergence of the MI simulation to the standard solution was evaluated by the error norm in the convergent state and the time constant in the transient state. Conditions investigated are shown in table 2. A feedback signal was applied at all grid points using all three velocity components (Case 1), or at all grid points but using partial components (Case 2), or at limited grid points using all velocity components (Case 3). The effect of the initial condition was also investigated in Case 1.

Table 2 Conditions of MI simulation

	Case 1	Case 2	Case 3
Feedback points	**All**	**All**	**Partial**
Feedback velocity components	**All**	**Partial**	**All**
Initial condition	**Independent solution and null velocity**	**Independent solution**	**Independent solution**

Table 3 Computational conditions

Periodical length L	**4**
Pressure difference δ_p	**0.0649**
Standard Reynolds number R_{e0} ($R_{e\tau}$)	**9000 (573)**
Grid points $N_1 \times N_2 \times N_3$	**80×40×40**
Grid spacing $h_1 \times h_2 \times h_3$	**0.05×0.025×0.025**
Time step h_T	**0.025**
Total residual at convergence	**0.015**
CPU time [s] for one time step	**10.4**

Standard solution and ordinary simulation without feedback

This section explains the standard solution and the ordinary simulation. The present computer code, ROTFLO2, was validated in detail in former studies [23, 25]. For a fully developed turbulent flow with the same geometry, the authors have previously examined the convergence of the solution with grid refinement [23]. Under the computational conditions summarized in Table 3, we obtained a proper turbulent flow solution in good agreement with the DNS solution by Huser & Biringen [22] in the mean u_1-velocity profile, the Reynolds stress distribution, and the energy spectrum of u_1-velocity perturbation [23] (see Fig. 5).

A standard solution was first obtained as a model of a real turbulent flow. The final velocity field of the statistically steady solution for a fully developed turbulent flow in the former study [23] was used as the initial condition of the standard solution.

The present study focused on the convergence of the solution of the MI simulation to the standard solution. The initial condition of the MI simulation was defined as the state of the standard solution at t = 20 (we confirmed that the autocorrelation function of the velocity fluctuation at the center of a cross section sufficiently reduces at t = 10). The two solutions are very different although their statistical properties are the same. This initial condition is used in most of the following MI simulations except for the special case of the null velocity condition.

MI simulation with feedback of full velocity components

A numerical experiment for MI simulation was performed using the above-mentioned standard solution as the model of real turbulent flow. The feedback signal in the MI simulation in this section was applied at all grid points as the artificial force vector in the discretized Navier-Stokes equation proportional to the difference in velocity vector between the standard solution and the simulation, and as the source term in the pressure equation (Case 1 in Table 2). MI simulation for the feedback signal determined with partial information of velocity components (Case 2) or partial grid points (Case 3) are considered in the following sections.

MI simulation was performed for various values of the feedback gain K_u, which represents diagonal components of the diagonal matrix $\mathbf{K_u}$. In order to evaluate the error of the MI simulation from the standard solution, we define the error norm $E_\mathbf{u}$ and E_p as follows:

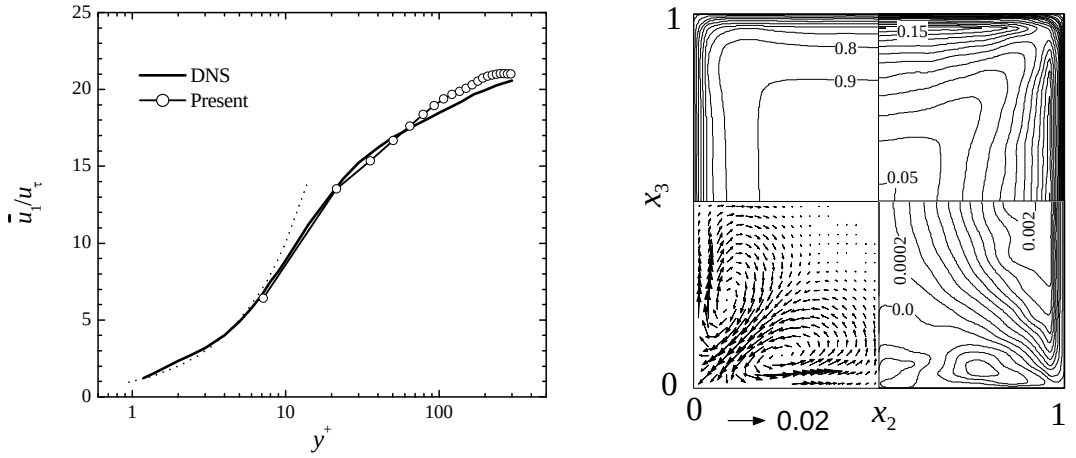

Fig. 5 (a) Comparison of mean axial velocity profile with DNS solution (Huser & Biringen 1993), and (b) Flow structure on a cross section for the present numerical solution for a fully developed turbulent flow through a square duct (Hayase 1999). Upper left: mean u_1-velocity contours normalized by the mean center velocity u_c; lower left: mean transverse velocity vectors normalized by the mean center velocity u_c; upper right: contours of RMS value of u_1-velocity fluctuation, $(\overline{u_1'^2})^{1/2}/u_c$; lower left: contours of the Reynolds stress, $\overline{u_1' u_2'}/u_c^2$

$$\begin{cases} E_{\mathbf{u}} = \left[\dfrac{1}{3N} \displaystyle\sum_{n=1}^{3N} \left(u_n - u_n^* \right)^2 \right]^{1/2} \\ E_p = \left[\dfrac{1}{N} \displaystyle\sum_{n=1}^{N} \left(p_n - p_n^* \right)^2 \right]^{1/2} \end{cases}, \tag{21}$$

where u_n denotes a component of $\mathbf{u}_N$, or u_1, u_2, u_3 at any grid point.

Variations of the error norms $E_{\mathbf{u}}$ and E_p for MI simulations with different values of the feedback gain K_u are plotted in Fig. 6. For the error norm of the velocity vector field in Fig.6 (a), the result for $K_u = 0$, corresponding to the ordinary simulation, remains almost constant ($E_0 = 0.13 \pm 0.02$) showing that the standard solution and the solution of the ordinary simulation maintain the same distance in the state space. In a range of the feedback gain, the error norm is reduced almost exponentially and afterwards deviates irregularly within some range. The exponential reduction rate in the transient stage increases with the feedback gain for $K_u \leq 32$, but becomes negative (meaning that the error increases) for $K_u = 64$, showing instability characteristics which are typical in feedback systems. The range of deviation of the error norm in the steady stage is almost constant with time for each gain. By carefully examining the variation of the error norm in that range, the error norm is seen to switch between two typical states near the bottom and top of the range: a quasi-stationary state near the bottom and a steady oscillation state near the top. The level of the bottom state, which takes the minimum value around 1×10^{-6} for $K_u = 2$, increases with increasing gain. The level of the top state, which gives the accuracy of the MI simulation, first decreases with increasing gain and remains almost constant for $K_u = 2$ and 8, but increases rapidly with further increases of the gain, and for $K_u = 64$ it becomes ten times larger than the error norm of the ordinary simulation. It is noted that the time of the bottom state or the top state seems to be correlated among the results of different feedback gains. This can probably be ascribed to the stability of the feedback system dependent on the standard solution, but further examination should be made in a future study.

The results for the error norm of the pressure field shown in Fig.6 (b) are qualitatively the same as those of the velocity vector field mentioned above. This is a natural consequence of convergence of MI simulation in the velocity field resulting in convergence in the pressure field. Therefore, we mainly focus on the velocity field in the followings.

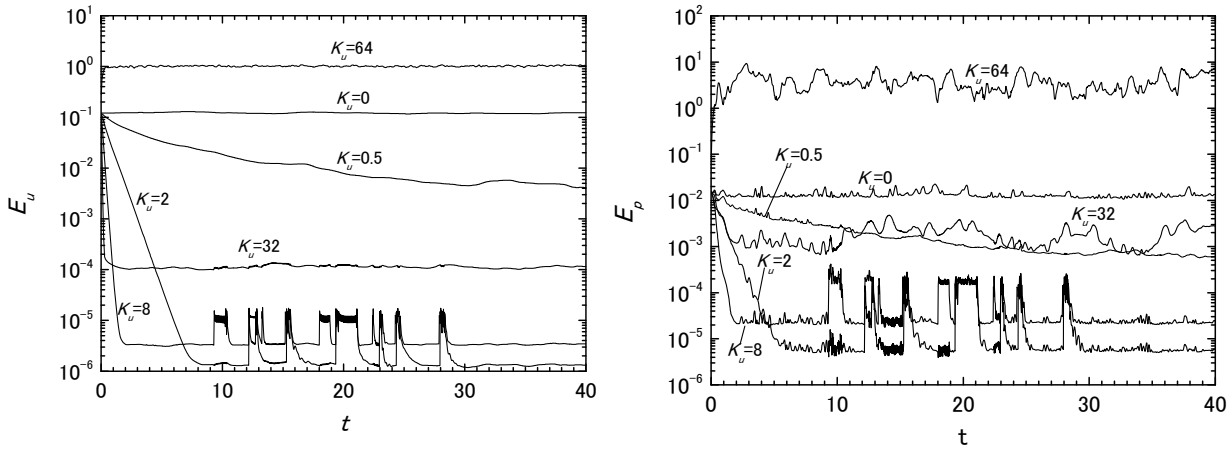

(a) **(b)**

Fig. 6 Variation of error norm of MI simulations with different feedback gains for (a) velocity, and (b) pressure.

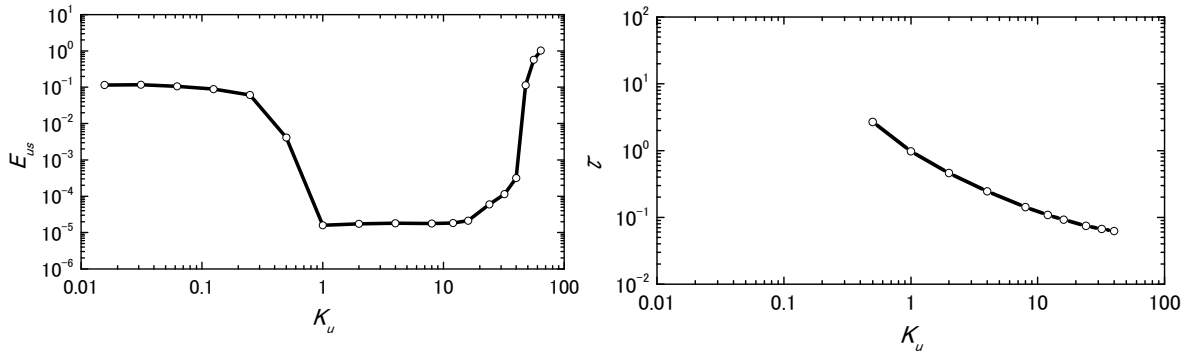

(a) **(b)**

Fig. 7 Variation of (a) steady error norm, and (b) time constant of MI simulation with the feedback gain.

The steady state error and time constant of the MI simulation obtained from the above results are plotted with the feedback gain in Fig. 7 (a) and (b), respectively. Steady state error in Fig.7(a) is determined as the maximum value of the error norm in the steady stage for $t \leq 40$ if the steady stage exists or the error norm at $t = 40$ otherwise. It is noted that the steady state error defined here gives the error bound of the MI simulation. Fig.7 (a) shows that a significant reduction of the error norm by a factor on the order of 10^{-4} is achieved in a range of the feedback gain of $1 \leq K_u \leq 16$. For larger feedback gains, the error norm gradually increases up to $K_u = 40$ and then suddenly increases and exceeds the error norm of the ordinary simulation. Stability analysis of the present feedback system remains as a future work. It is noted that the results for feedback gains smaller than 1 do not show the error norm in the steady stage as mentioned above. However, this is not important since little advantage is expected by using feedback gains which are too small. The time constant in Fig.7 (b) is determined as the time in which the excess of the error norm from its steady value decreases to 37 %, or e^{-1}, of its initial value [16]. The time constant decreases almost inversely proportional to the feedback gain in a range of $0.5 \leq K_u \leq 40$.

In order to evaluate the influence of different initial conditions in the whole domain, variation of error norms for the above results are plotted in Fig. 8. The figure also includes the result for when the feedback was terminated

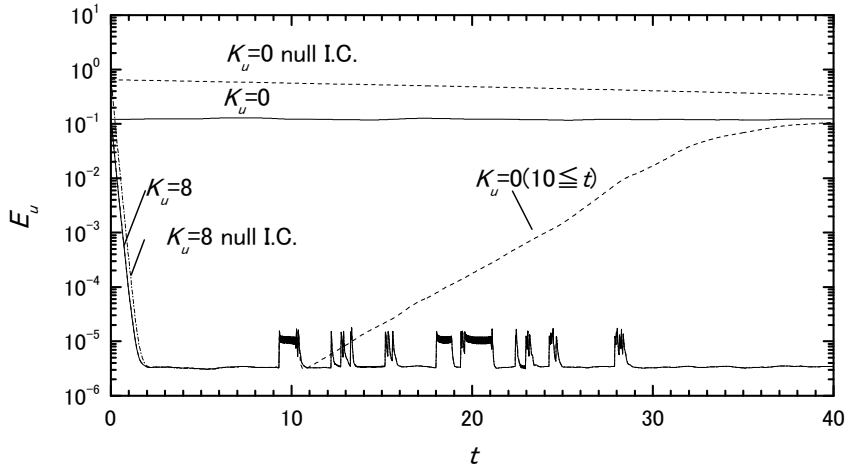

Fig. 8 Variation of the error norm for MI simulations with different initial conditions and when case feedback was terminated at t = 10.

in the middle of the calculation at $t = 10$. In the figure, the error norms for the ordinary simulations from the two relevant initial conditions are also plotted for purposes of comparison. It is noted that the ordinary simulation from the null initial velocity corresponds to the MI simulation with a feedback gain $K_u = 0$. Its error norm decreases to the level of the other ordinary simulation as it converges to the fully developed turbulent flow solution in a large amount of time as expected in the figure. By comparing two MI simulations having different initial conditions, the error norms are seen to decrease at the same exponential rate, and interestingly, come to have the same steady values with irregular perturbation ranging between 7×10^{-6} and 1.5×10^{-5}.

The MI simulation after termination of the feedback at $t = 10$ is identical to the ordinary simulation starting from the initial condition very close to the standard solution. Its error norm stays in a range of the MI simulation for a short time but then increases exponentially. This exponential rate is considered to be a structural instability characteristic of the relevant turbulent flow by which a small difference in initial condition diverges exponentially. This is the reason why ordinary simulation is incapable of reproducing the instantaneous structure of the relevant turbulent flow over a long period of time. In the MI simulation, on the other hand, the feedback loop modifies the dynamical structure of the system. The computational results from different initial conditions converge exponentially to the standard turbulent flow solution and stay close to it within a distance in the state space.

MI simulation with feedback of partial velocity components

In the former section, it was revealed that the MI simulation converged to the standard solution when the feedback signal proportional to the error in velocity vector was applied to the governing equations at the all grid points. In this section we consider the case in which the feedback signal includes partial velocity components: two velocity components u_1 and u_3 (by omitting one transverse velocity component), or u_2 and u_3 (omitting the primary velocity component), or one velocity component u_1 or u_2 (Case 2 in Table 2). It is noted that the other cases using two components u_1 and u_2, and one component u_3 are omitted considering the symmetry of the problem.

The steady state error and time constant of the MI simulation for each case are plotted with feedback gain in Fig. 9 (a) and (b), respectively. The former results using all three velocity components are also included in the figures for reference. Steady state error in Fig. 9 (a) is determined in the same way in Fig.7 (a). The result using u_1 and u_2 velocity components by omitting one transverse velocity component u_3 is somewhat degraded in comparison with that of the former case using all three velocity components, but still achieves sufficient reduction of the error by a factor of 10^{-4}. The other results using two velocity components, u_2 and u_3, and one component, u_1 or u_2, are all substantially degraded in comparison with the former two cases, although the unstable behavior for $K_u > 40$ is similar in all cases. Comparison of the time constants in Fig. 9 (b) shows a similar result as mentioned above. The result using u_1 and u_2 velocity components is almost comparable to that of the case using all three velocity components, but the time constants for the other cases are more than ten times larger implying slow convergence.

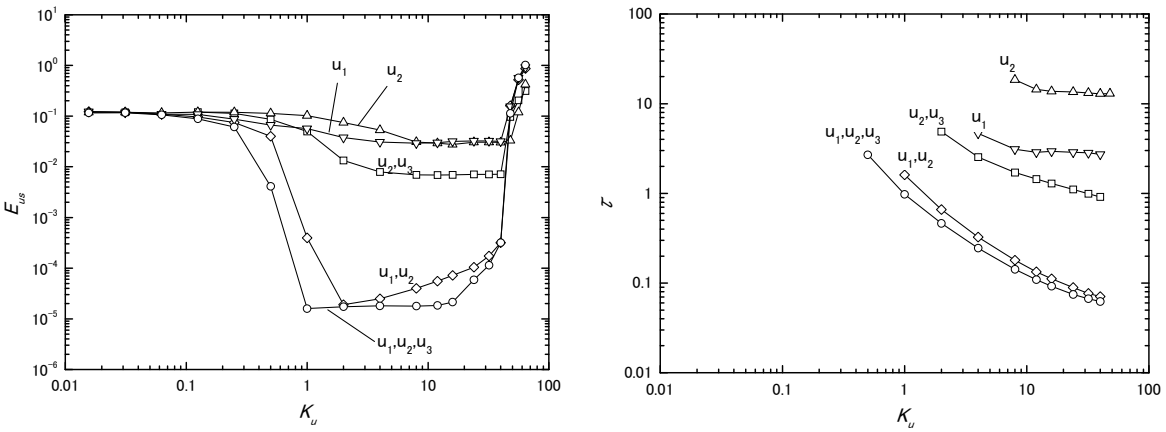

Fig. 9 Variation with gain for (a) steady error norm, and (b) time constant of MI simulations with the feedback of partial velocity components.

MI simulation with feedback at partial points

In the former section, it was revealed that MI simulation with the feedback at all grid points but using two velocity components by omitting one transverse velocity component showed a good result, while the other cases using other combinations of partial velocity components did not. In this section we consider the case in which the feedback signal is determined from all three velocity components but applied at limited grid points in the domain (Case 3 in Table 2). We perform MI simulations applying the feedback at the grid points on the planes skipped in the x_1 direction or those skipped in the x_2 direction.

Figure 10 and Figure 11 show the steady state error and the time constant of the MI simulation in which the feedback signal determined with all three velocity components was applied on selected planes in the x_1 direction or x_2 direction. As expected from the former results, reduction of the feedback points in the x_1 direction did not seriously influence the steady state error, as shown in Fig.10 (a). For example, feedback on the planes with a density of 1/20 of the whole domain still reduced the error by a factor on the order of 10^{-4} from the ordinary simulation if the gain is optimized for that condition. In Fig. 10 (b), however, the time constant increased monotonically with decreasing density of the planes. The results of MI simulation were seriously degraded

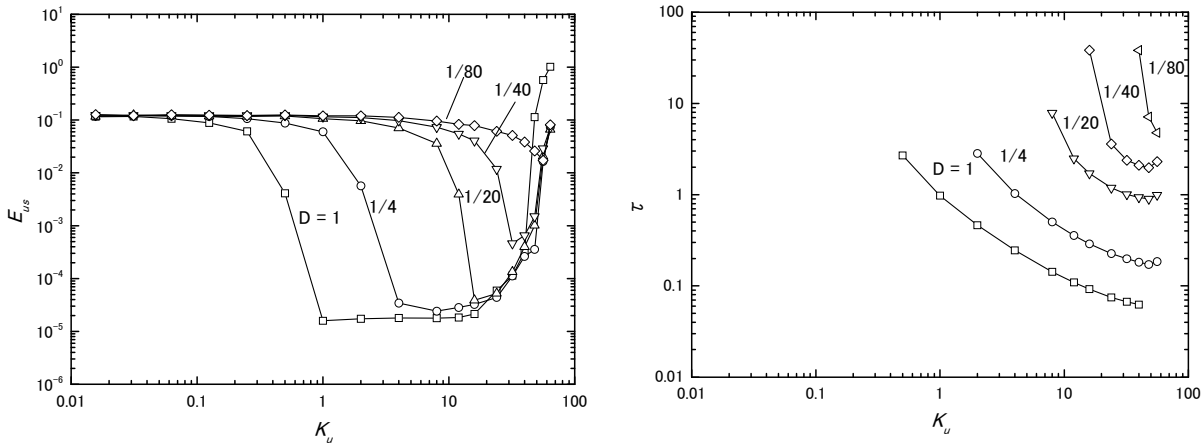

Fig. 10 Variation with gain for (a) steady error norm, and (b) time constant of MI simulations with the feedback at the grid points on the planes skipped in the x_1 direction.

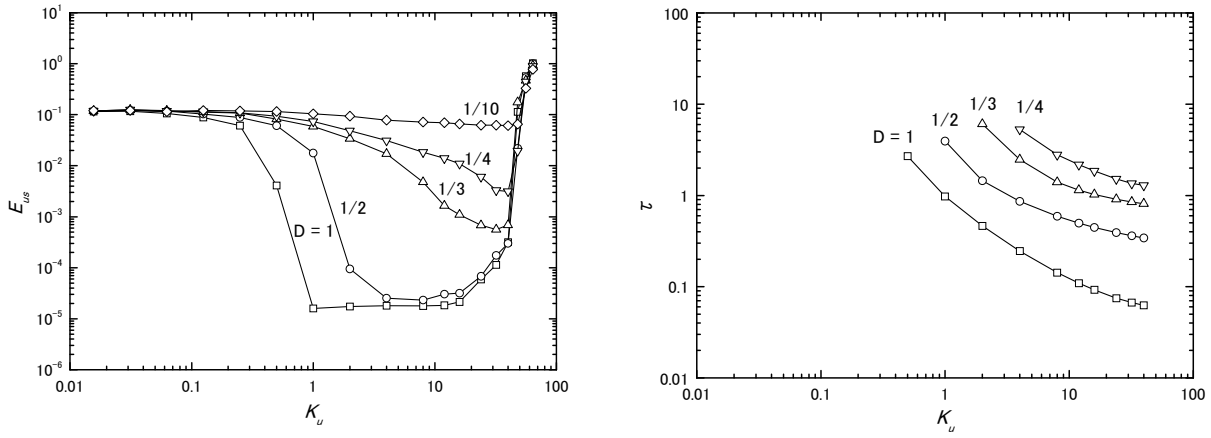

Fig. 11. Variation with gain for (a) steady error norm, and (b) time constant of MI simulations with the feedback at the grid points on the planes skipped in the x_1 direction.

when the feedback points were reduced in the x_2 direction as shown in Fig. 11 (a). For example, the density of planes necessary to maintain the reduction of the error by the order of 10^{-4} is 1/2, which is ten times larger than that of the former case of skipping in the x_1 direction. The time constant increased monotonically with decreasing density of the planes.

Eigenvalue analysis

In the followings a numerical experiment is performed to examine the validity of the eigenvalue analysis presented in the previous section. Eigenvalue analysis and MI simulation are performed for the case of simple model turbulent flow through a square duct with feedback using all three velocity components (Case (A)), or using the mainstream and one transverse velocity component (Case (B)) (see Table 4).

In the numerical experiment, we deal with a numerical solution for a fully developed turbulent flow in a square pipe as a model of real flow, or a standard solution. The computational conditions are shown in Table 5. Although the grid resolution is not fine enough to correctly simulate the detailed structure of the turbulent flow, the numerical solution has the fundamental characteristics of the relevant turbulent flow [23]. This simplification is justified because the purpose of this numerical experiment is not to investigate the turbulent flow but to examine whether the eigenvalue analysis can be used to design the MI simulation.

In the following, all the values are expressed in dimensionless form using the side length of the square cross section $\tilde{b}$, the density of fluid $\tilde{\rho}$, and the mean axial velocity $\tilde{u}_{m0}$ given by $\tilde{u}_{m0} = \sqrt{2\Delta\tilde{p}/\lambda L}$ where the coefficient of resistance λ is evaluated by means of Blasius' formula [24] $\lambda = 2\Delta p/L = 0.316R_{e0}^{-1/4}$. Time scale is given by $\tilde{b}/\tilde{u}_{m0}$. As to the boundary condition, periodical velocity condition and the constant pressure difference δ_p corresponding to a specified Reynolds number $R_{e0} = \tilde{u}_{m0}\tilde{b}/\tilde{\nu}$ is assumed between the upstream and downstream boundaries for a duct with a periodical length of 4. A non-slip condition is assumed on the walls [6].

Computational scheme used in this study is the same as that in former section. The discretized representations of the governing equations are obtained through the finite volume method on an orthogonal equidistant staggered grid system. Convection terms are discretized by a reformulated QUICK scheme. A two-time level implicit scheme is used for time dependent terms. The resultant set of finite difference equations is solved using the iterative procedure based on the SIMPLER method.

The standard solution or the model of the real flow was obtained using the final result of the statistically steady flow solution for a fully developed turbulent flow as the initial condition. As to the MI simulation considered here, we use a computational scheme identical to that for the standard solution. The feedback gain matrix $\mathbf{K_u}$ in Eq. (9) is assumed to be a diagonal matrix whose diagonal components are all of identical value k_u:

Table 4 Conditions of MI simulation

	Case A	Case B	Case C
Simulation	**Ordinary**	**MI**	**MI**
Feedback points	**None**	**All**	**All**
Feedback velocity components	**None**	**All (u_1, u_2, u_3)**	**Partial (u_1, u_2)**

Table 5 Computational conditions

Periodical length L	**4**
Pressure difference	**0.0649**
Standard Reynolds number	**9000**
Grid points	**20×10×10**
Time increment	**0.025**
Total residual at convergence	**0.01**

$$\mathbf{K_u} = k_u \mathbf{I} \quad . \tag{22}$$

Hereafter, the orthogonal component k_u is called the feedback gain. The resultant feedback signal accelerates or

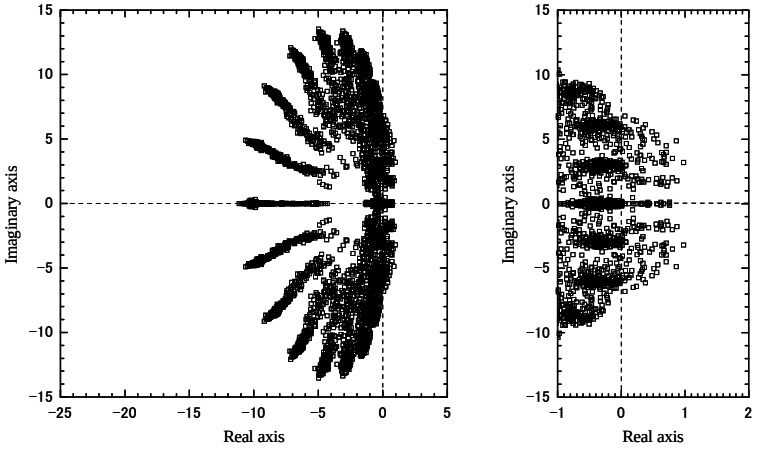

Fig.12 Eigenvalue distribution of ordinary simulation (case A)

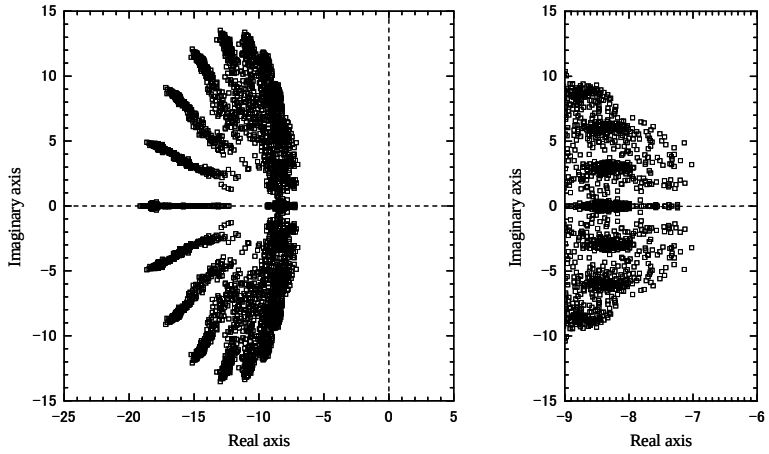

(a) Case B

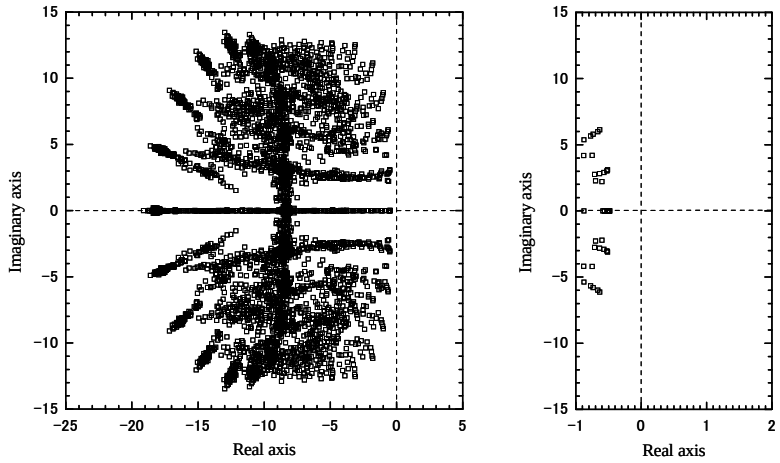

(b) Case C

Fig. 13 Eigenvalue distribution of MI simulations (ku=8)

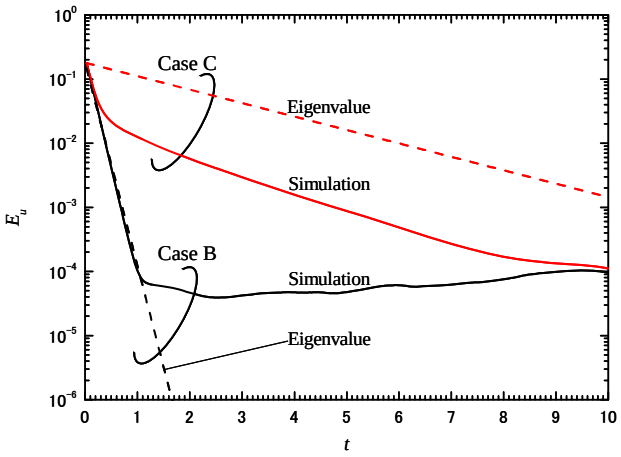

Fig. 14 Comparison of variation of error norm between eigenvalue analysis and numerical simulation

decelerates the fluid in a control volume to reduce the error in velocity. As for $\mathbf{C_u}$ in Eq. (9), we consider two cases: all three velocity components, or the mainstream and one transverse velocity component are available at all the grid points.

As to the eigenvalue analysis, we assume no measurement error. Terms due to model errors are also ignored since we use the same computational scheme for both the standard solution and MI simulation canceling out the model error terms in Eqs. (10) and (11). For calculation of system matrix **A'** in Eq. (18), $\tilde{B}$ in Eq. (16) is numerically obtained from singular value decomposition by using MATLAB R2006b (ver7.3, The MathWorks). The expression of matrix A is similar to the expression of the basic equation of the SIMPLER method (omitted due to space limitation). The eigenvalues of matrix **A'** are calculated by the QR method by using SCSL library. Computation using MATLAB was performed with SX-9 in Cyberscience Center, Tohoku University, and other computation was performed with Altix 3700 Bx2 using one CPU in the Advanced Fluid Information Research Center, Institute of Fluid Science, Tohoku University.

In the following we consider three cases: case (A), ordinary simulation; case (B), MI simulation with feedback using all three velocity components; and case (C), MI simulation with feedback using the mainstream and one transverse velocity component (see Table 4).

Eigenvalues, λ_i (i=1,2,・・・,2N,N=2000) of the system matrix A' of the error dynamics for the ordinary simulation are shown in Fig. 12. The right figure of Fig.12 is a figure whose real axis is enlarged to show the most unstable eigenvalues. For ordinary simulation, a number of eigenvalues are unstable, the most unstable eigenvalues being λ_m=0.98±3.2j. This means that the numerical simulation starting from an initial condition near the standard solution deviates from it exponentially, representing a sensitive dependence on the initial condition, which is typical for turbulent flows.

Figures 13 (a) and (b) show the eigenvalues for MI simulation of cases (B) and (C) with feedback gain k_u = 8. In each case, all eigenvalues have a negative real part, implying that the error dynamics is stable due to the effect of feedback, and the error of the MI simulation decreases exponentially. The result for case (B) in Fig. 13 (a) is a translation of the result of Fig. 12 in the negative real direction with an amount of the feedback gain k_u. This is obvious from the definition of A in Eq. (13). The least stable eigenvalues are λ_m=-7.02±3.2j (see right figure of Fig. 13 (a)). In the result for case (C) in Fig. 13 (b), the eigenvalues also shift to the left, but the amount of the shift is less than in case (B) for some eigenvalues. The least stable eigenvalues are λ_m=-0.48±0.029j (see right figure of Fig. 13 (b)) .

In the following, the results of the eigenvalue analysis and MI simulation are shown and compared. Here, the norm of velocity error is defined as

$$E_u \equiv \left[\frac{1}{3N} \mathbf{e_u}^T \mathbf{e_u} \right]^{1/2} \tag{23}$$

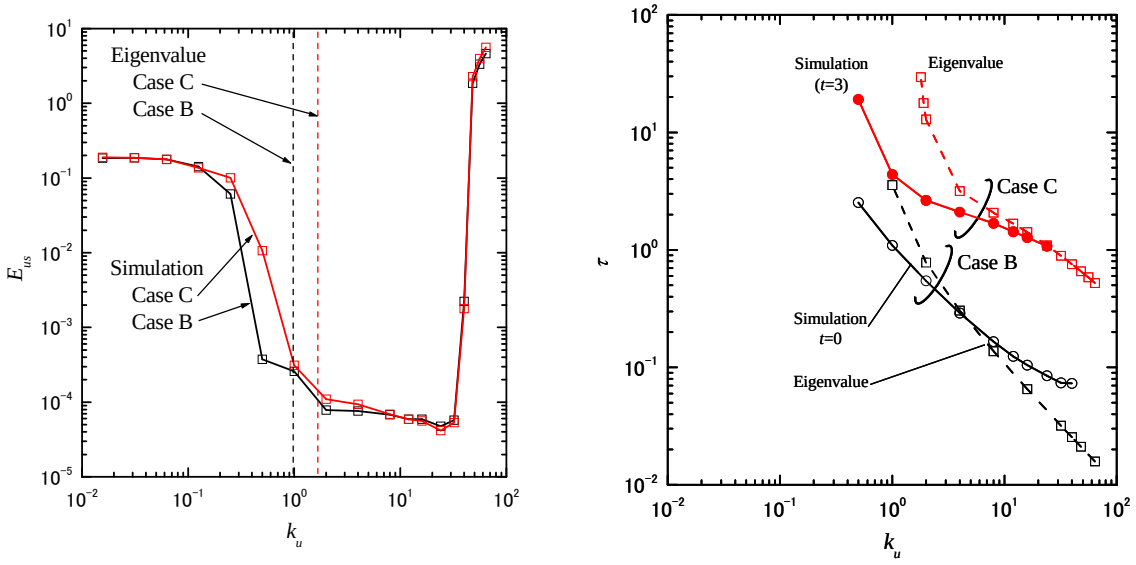

Fig.15 Steady error norm and time constant with feedback gain

Time-variation of the error norm E_u for the MI simulation with the feedback gain $k_u = 8$ in the cases of (B) and (C) are indicated in Fig. 14 by the solid lines. In case (B), the error norm first decreases exponentially and then remains in a certain range. On the other hand, in case (C), the error norm first decreases exponentially in the same way as in case (B), but the reducing rate changes around $t = 0.6$ and the error decreases more slowly afterwards. Broken lines in the figure represent the variation of the error norm for the least stable mode obtained from the eigenvalue analysis for cases (B) and (C). These are calculated using the real part of the eigenvalue and the initial magnitude identical to that of the MI simulation.

In MI simulation, the error norm reaches some steady value as time passes. Fig. 15 (a) shows steady error with the feedback gain. As shown in this figure, the steady error norm E_{us} decreases to order of 10^{-4} in the range of $0.5<k_u<24$ for case (B) or $1< k_u <24$ for case (C), respectively. The broken lines correspond to the critical feedback gain, or the lower limit of the feedback gain, below which there exist unstable eigenvalues. The error norm increases with excessive feedback gain above 30 in the MI simulation. This result is possibly explained by the discrete-time system analysis, and is beyond the scope of present paper.

Next, we consider the time constant τ as the time in which the error norm decreases by a factor of $1/e$. In MI simulation, as shown in Fig. 14, the rate of the error norm reduction is almost constant for case (B), while it changes around $t = 0.6$ for case (C). We evaluated the time constant at $t = 0$ for case (B), or the value at $t = 3$ for case (C). For eigenvalue analysis, the time constant τ of E_u is estimated as

$$\tau = -\frac{1}{\lambda_k}, \tag{25}$$

where λ_k is the real part of the eigenvalue for the least stable mode. Generally, as time passes, the least stable mode becomes the dominant mode.

The variation of the time constant with the feedback gain is compared between the MI simulation and the eigenvalue analysis for cases (B) and (C) in Fig. 15 (b). The results of eigenvalue analysis agree well with those of the MI simulation except for case (C) with small feedback gain below 4.

The time required for calculation of the 2000 dimensional eigenvalues was about 30 minutes while the corresponding computation of MI simulation was about 7 minutes. Large computational time to obtain eigenvalues of large dimensional system is an inherent problem of the proposed method, and will be treated in a future work.

Summary

In this article formulation of MI simulation and equations of linearized error dynamics and eigenvalue analysis of MI simulation were explained. Example of MI simulation was presented for a fully developed turbulent flow in a square duct. Numerical experiment was performed for MI simulation with a feedback signal from the predetermined standard turbulent flow solution. Convergence of MI simulation to the standard solution was investigated as a function of feedback gain and spatial and temporal density of feedback signal. Eigenvalue analysis was performed to examine the validity of the linearized error dynamics approach in the design of feedback signal.

References

[1] Thompson JMT, Stewart HB. Nonlinear Dynamics and Chaos. John Wiley and Sons; 1986.

[2] Benjamin SG, Dévényi D, Weygandt SS, Brundage KJ, Brown JM, Grell GA, Kim D, Schwartz BE, Smirnova TG, Smith TL, Manikin GS. An Hourly Assimilation-Forecast Cycle. The RUC Mon Wea Rev 2004; 132:495-518.

[3] Talagrand O. A study of the Dynamics of Four Dimensional Data Assimilation. Tellus 1981; 33: 43-60.

[4] Zupanski M. Regional 4-Dimensional Variational Data Assimilation in a Quasi-Operational Forecasting Environment. Mon Wea Rev 1993; 121: 2396-2408.

[5] Bouttier F, Rabier F. The Operational Implementation of 4D-VAR. ECMWF Newsletter 1997; 78: 2-5

[6] Humphrey JAC, Devarakonda R, Queipo N. Interactive Computational-Experimental Methodologies (ICEME) for Thermofluids Research: Application to the Optimized Packaging of Heated Electronic Components. Computers and Computing in Heat Transfer Science and Engineering, (ed. Yang, K. T. and Nakayama, W.). CRC Press and Begell House. New York. 1993; 293-317.

[7] Zeldin BA, Meade AJ. Integrating experimental data and mathematical models in simulation of physical systems. AIAA J 1997; 35:1787-1790.

[8] Ido T, Murai Y, Yamamoto F. Postprocessing Algorithm for Particle-Tracking Velocimetry Based on Ellipsoidal Equations. Exp in Fluids 2002; 32:326-336.

[9] 9. Uchiyama M, Hakomori K. Measurement of Instantaneous Flow Rate Through Estimation of Velocity Profiles. IEEE Trans Automat Contr 1983; AC-28; 380-388.

[10] Sorenson H, ed. Kalman filtering: theory and application. IEEE press; 1985.

[11] Högberg M, Bewley TR, Henningson DS. Linear feedback control and estimation of transition in plane channel flow. J Fluid Mech 2003;481:149-175.

[12] Hayase T, Hayashi S. State Estimator of Flow as an Integrated Computational Method with the Feedback of Online Experimental Measurement. Trans ASME J Fluids Eng 1997; 119(4):814-822.

[13] Nisugi K, Hayase T, Shirai A. Fundamental Study of Hybrid Wind Tunnel Integrating Numerical Simulation and Experiment in Analysis of Flow Field. JSME Int J Ser B 2004; 47(3):593-604.

[14] Hayase T, Nisugi K, Shirai A. Numerical Realization for Analysis of Real Flows by Integrating Computation and Measurement. Int J Num Meth Fluids 2005; 47: 543-559.

[15] Funamoto K, Hayase T, Shirai A, Saijo Y, Yambe T. Fundamental study of Ultrasonic-Measurement-Integrated simulation of real blood flow in the aorta. Ann Biomed Eng 2005; 33: 413-426.

[16] Skelton RE. Dynamic Systems Control. John Wiley & sons; 1988.

[17] Misawa EA, Hedrick JK. Nonlinear Observers: A State-of-the-art Survey. J Dynamic Sys Meas Control Trans ASME 1989; 111: 344-352.

[18] Curtain RF, Zwart HJ. An Introduction to Infinite-Dimensional Linear Systems Theory. Springer- Verlag, New York; 1995: 246.

[19] Li X, Yong J. Optimal Control Theory for Infinite Dimensional Systems, Birkhäuser; 1995.

[20] Imagawa K, Hayase T, Eigenvalue analysis of linearized error dynamics of measurement integrated flow simulation, Computers & Fluids 2010; 39, 1796-1803.

[21] Imagawa K, Hayase T, Numerical experiment of measurement-integrated simulation to reproduce turbulent flows with feedback loop to dynamically compensate the solution using real flow information, Computers & Fluids 2010; 39, 1439-1450.

[22] Huser A, Biringen S. Direct Numerical Simulation of Turbulent Flow in a Square Duct. J Fluid Mech 1993; 257: 65-95.

[23] Hayase T. Monotonic Convergence Property of Turbulent Flow Solution With Central Difference and Quick Schemes. Trans ASME J Fluids Eng 1999; 121(2):351-358.

[24] Schlichting H. Boundary-Layer Theory 7th edition. McGraw-Hill. New York. 1979.

[25] Hayase T, Humphrey JAC, Greif R. A Consistently Formulated QUICK Scheme for Fast and Stable Convergence Using Finite-Volume Iterative Calculation Procedures. J Compt Phys 1992; 98:108-118.

[26] Fletcher CAJ. Computational Techniques for Fluid Dynamics. Springer-Verlag 1988:302.

[27] Patankar SV. Numerical Heat Transfer and Fluid Flow. Hemisphere. Washington DC/New York. 1980.